THE ASTROPHYSICAL JOURNAL, 545:86–99, 2000 December 10
© 2000. The American Astronomical Society. All rights reserved. Printed in U.S.A.

ESCAPE OF IONIZING RADIATION FROM HIGH-REDSHIFT GALAXIES

KENNETH WOOD[1] AND ABRAHAM LOEB[2]
Harvard-Smithsonian Center for Astrophysics, 60 Garden Street, Cambridge, MA 02138
Received 1999 November 16; accepted 2000 July 16

ABSTRACT

We use a three-dimensional radiation transfer code to calculate the steady state escape fraction of ionizing photons from disk galaxies as a function of redshift and galaxy mass. The gaseous disks are assumed to be isothermal (with a sound speed $c_s \sim 10$ km s^{-1}) and radially exponential. Their scale radius is related to the characteristic spin parameter and virial radius of their host halos, and their vertical structure is dictated by their self-gravity. The sources of radiation are taken to be either stars embedded in the disk or a central quasar. The predicted increase in the disk density with redshift results in an overall decline of the escape fraction with increasing redshift. For typical parameters of smooth disks, we find that the escape fraction at $z \sim 10$ is $\lesssim 1\%$ for stars but $\gtrsim 30\%$ for miniquasars. Unless the smooth gas content of high-redshift disks was depleted by more than an order of magnitude due to supernovae-driven outflows or fragmentation, the reionization of the universe was most likely dominated by miniquasars rather than by stars.

Subject headings: galaxies: formation — H II regions — quasars: general

1. INTRODUCTION

Recently, there has been considerable theoretical interest in calculating the reionization history of the intergalactic medium (e.g., Haiman & Loeb 1997; Abel, Norman, & Madau 1999; Madau, Haardt, & Rees 1999; Miralda-Escudé, Haehnelt, & Rees 2000; Gnedin 2000). The intergalactic ionizing radiation field is an essential ingredient in these calculations and is determined by the amount of ionizing radiation escaping from the host galaxies of stars and quasars. The value of the escape fraction as a function of redshift and galaxy mass remains a major uncertainty in all current studies and could affect the cumulative radiation intensity by orders of magnitude at any given redshift. In general, the gas density increases toward the location of galaxies in the intergalactic medium (IGM), and so the transfer of the ionizing radiation must be followed through the densest regions on the galactic length scales. Reionization simulations are limited in dynamical range and small-scale resolution and often treat the sources of ionizing radiation (quasars and galaxies) as unresolved point sources within the large-scale intergalactic medium (see, e.g., simulations by Gnedin 2000). In this paper we calculate the escape of ionizing photons from disk galaxies as a function of formation redshift and mass, thereby providing a means of estimating the ionizing luminosity input for simulations of reionization.

The escape of ionizing radiation ($h\nu > 13.6$ eV, $\lambda < 912$ Å) from the disks of present-day galaxies has been studied in recent years in the context of explaining the extensive diffuse ionized layers observed above the disk in the Milky Way (Reynolds et al. 1995) and other galaxies (e.g., Rand 1996; Hoopes, Walterbos, & Rand 1999). Theoretical models predict that of order 3%–14% of the ionizing luminosity from O and B stars escapes the Milky Way disk (Dove & Shull 1994; Dove, Shull, & Ferrara 2000). A similar escape fraction of $f_{\rm esc} = 6\%$ was determined by Bland-Hawthorn & Maloney (1999) based on Hα measurements of the Magellanic Stream. From Hopkins Ultraviolet Telescope observations of four nearby starburst galaxies (Leitherer et al. 1995; Hurwitz, Jelinsky, & Dixon 1997), the escape fraction was estimated to be in the range $3\% < f_{\rm esc} < 57\%$. If similar escape fractions characterize high-redshift galaxies, then stars could have provided a major fraction of the background radiation that reionized the IGM (Madau & Shull 1996; Madau 1999). However, the escape fraction from high-redshift galaxies, which formed when the universe was much denser [$\rho \propto (1+z)^3$], may be significantly lower than that predicted by models that are adequate for present-day galaxies.

In popular cold dark matter (CDM) models, the first stars and quasars formed at redshifts $z \gtrsim 10$ (see, e.g., Haiman & Loeb 1997, 1998; Gnedin 2000). These sources are expected to have formed in galaxies where the gas has cooled significantly below its virial temperature and has assembled into a rotationally supported disk configuration (Barkana & Loeb 1999, 2000). The ionizing radiation leaving their interstellar environments, and ultimately their host galaxies, streamed into intergalactic space creating localized ionized regions. Through time these ionized regions, or "Strömgren volumes," expanded and eventually overlapped at the epoch of reionization (Arons & Wingert 1972). The redshift of reionization is still unknown, but the detection of flux shortward of the Lyα resonance for galaxies out to redshifts $z \sim 5$–6 (Stern et al. 2000; Weymann et al. 1998; Dey et al. 1998; Spinrad et al. 1998; Hu, Cowie, & McMahon 1998; Hu, McMahon, & Cowie 1999) implies that reionization occurred at even higher redshifts (Gunn & Peterson 1965).

Current reionization models assume that galaxies are isotropic point sources of ionizing radiation and adopt escape fractions in the range $5\% < f_{\rm esc} < 60\%$ (see, e.g., Gnedin 2000; Miralda-Escudé et al. 2000). In this paper, we examine the validity of these assumptions by following the radiation transfer of ionizing photons in the gaseous disks of high-redshift galaxies. We consider either stars or a central quasar as the source of ionizing photons. The mass and radial extent of the gaseous galactic disks, in which these sources are embedded, are functions of redshift and can be related to the mass and radius of their host dark

[1] kenny@claymore.harvard.edu.
[2] aloeb@cfa.harvard.edu.

matter halos (Navarro, Frenk, & White 1997; Mo, Mao, & White 1998). The vertical structure of the disk is dictated by its self-gravity and will be assumed to follow the isothermal profile (Spitzer 1942) with a thermal (or turbulent) speed of ~ 10 km s^{-1} for all galaxies. This corresponds to the characteristic thermal speed of photoionized gas and also to an effective gas temperature of $\sim 10^4$ K, below which atomic cooling is suppressed (Binney & Tremaine 1987). We relate the ionizing luminosity emitted by the stars or quasars to the mass of the host dark matter halos (Haiman & Loeb 1997, 1998), adopting current estimates for Lyman continuum production in starburst galaxies (Leitherer et al. 1999) and quasars (Laor & Draine 1993). The escape fractions for disk galaxies as a function of mass and redshift are then calculated with a Monte Carlo radiation transfer code, similar to that of Och, Lucy, & Rosa (1998).

Our numerical code finds the ionized fraction of the gas and follows the associated radiation transfer of the ionizing photons in a steady state. Strictly speaking, it provides an upper limit on the degree of ionization and the corresponding escape fraction for a given source luminosity. However, the characteristic propagation time of the ionization front through the scale height of the galactic disks of interest here ($\ll 10^6$ yr) is much shorter than the expected decay time of the starburst or quasar activities which produce the ionizing photons.

For the sake of simplicity, we begin our study of the problem with the assumption that the gas is distributed smoothly within the disk. Clumping is known to have a significant effect on the penetration and escape of radiation from an inhomogeneous medium (e.g., Boissé 1990; Witt & Gordon 1996, 2000; Neufeld 1991; Haiman & Spaans 1999; Bianchi et al. 2000). The inclusion of clumpiness will introduce several unknown free parameters into the calculation, such as the number and density contrast of the clumps, and the spatial correlation between the clumps and the ionizing sources. An additional complication might arise from hydrodynamic feedback, whereby part of the gas mass might be expelled from the disk by stellar winds and supernovae (Couchman & Rees 1986; Dekel & Silk 1986). We adopt a simple approach to gauge the significance of clumpiness in § 4 by modeling the galactic disk density as a two-phase medium (Witt & Gordon 1996, 2000) and calculate the escape fractions from such clumpy disks. We also simulate the effects of outflows and the possible expulsion of gas from the disk by reducing the mass of the smoothly distributed gas in the disk by an order of magnitude.

In § 2 we present the details of our model, including the disk geometry, the gas distribution, the source luminosities, and the radiation transfer code. Section 3 presents the results of our models in terms of the derived escape fractions. Our investigation into clumpy disks is presented in § 4. We conclude with a discussion of our findings in § 5.

2. MODEL INGREDIENTS

In order to determine the escape of ionizing photons, we need to specify the geometry and density of the disk galaxies as a function of their formation redshift, as well as the location and luminosity of the ionizing sources within the disks.

2.1. *Geometry*

We adopt the theoretical properties of disks forming within cold dark matter halos (Mo et al. 1998; Navarro et al. 1997). A dark matter halo of mass $M_{\rm halo}$ which forms at a redshift z_f is characterized by a virial radius (Navarro et al. 1997)

$$r_{\rm vir} = 0.76 \left(\frac{M_{\rm halo}}{10^8\ h^{-1}\ M_\odot} \right)^{1/3} \left(\frac{\Omega_0}{\Omega(z_f)} \frac{\Delta_c}{200} \right)^{-1/3} \times \left(\frac{1+z_f}{10} \right) h^{-1}\ {\rm kpc}\ , \quad (1)$$

where $H_0 = 100\ h$ km s^{-1} Mpc^{-1} is the Hubble constant, Ω_0 is the present mean density of matter in the universe in units of the critical density ($\rho_{\rm crit} = 3H_0^2/8\pi G$), and

$$\Omega(z_f) = \frac{\Omega_0 (1+z_f)^3}{\Omega_0 (1+z_f)^3 + \Omega_\Lambda + (1-\Omega_0-\Omega_\Lambda)(1+z_f)^2}\ ; \quad (2)$$

Δ_c is the threshold overdensity of the virialized dark matter halo which can be fitted by (Bryan & Norman 1998)

$$\Delta_c = 18\pi^2 + 82d - 39d^2 \quad (3)$$

for a flat universe with a cosmological constant, where $d = \Omega(z_f) - 1$.

We assume that the disk mass (stars plus gas) is a fraction m_d of the halo mass,

$$M_{\rm disk} = m_d M_{\rm halo}\ , \quad (4)$$

where $m_d = \Omega_b/\Omega_0$ and Ω_b is the present baryonic density parameter. We adopt $\Omega_0 = 0.3$ and $\Omega_b = 0.05$, giving $m_d = 0.17$. At the high redshifts of interest, most of the virialized galactic gas is expected to cool rapidly and assemble into the disk. Mo et al. (1998) suggest values in the range $0.05 < m_d < 1$. In our simulations in § 3.1, we also consider $m_d = 0.02$ which is an order of magnitude lower than our canonical value of $m_d = 0.17$. The exponential scale radius of the disk is given by (Mo et al. 1998)

$$R = \left(\frac{j_d}{\sqrt{2} m_d} \right) \lambda r_{\rm vir}\ , \quad (5)$$

where the disk angular momentum is a fraction j_d of that of the halo and the spin parameter λ is defined in terms of the total energy, $E_{\rm halo}$, and angular momentum, $J_{\rm halo}$, of the halo, $\lambda = J_{\rm halo} |E_{\rm halo}|^{1/2} G^{-1} M_{\rm halo}^{-5/2}$. For our calculation of the escape of ionizing radiation, we will adopt the values of $j_d/m_d = 1$ and $\lambda = 0.05$, yielding $R = 0.035 r_{\rm vir}$. These values provide a good fit to the observed size distribution of galactic disks, given the characteristic value of the spin parameter found in numerical simulations of halo formation (Mo et al. 1998 and references therein).

The vertical, z, structure of thin galactic disks is dictated by their self-gravity. For simplicity, we assume that the disk is isothermal and its surface density varies exponentially with radius. The number density of protons in the disk is then given by (Spitzer 1942)

$$n(r, z) = n_0\, e^{-r/R}\ {\rm sech}^2 \left(\frac{z}{\sqrt{2} z_0} \right), \quad (6)$$

where

$$z_0 = \frac{c_s}{(4\pi G \mu m_{\rm H}\, n_0\, e^{-r/R})^{1/2}} \quad (7)$$

is the scale height of the disk at radius r, μ is the atomic weight of the gas, and $m_{\rm H}$ is the mass of a hydrogen atom. Here $c_s = \sqrt{kT/\mu m_{\rm H}}$ is the sound speed (or the effective

turbulence speed), which dictates the scale height of the disk. We take $c_s = 10$ km s^{-1}, which corresponds to a gas temperature of $\sim 10^4$ K. This temperature is typical of photoionized gas and should characterize the galactic disks of interest here since the atomic cooling rate decreases strongly at lower temperatures. The combination of isothermality and the exponential radial profile results in a disk scale height that increases with radius (see eq. [7]). The galactic center number density, n_0, can be related to the total mass of the disk which is obtained by integrating the density over the entire disk volume,

$$n_0 = \frac{M_{\rm disk}}{\mu m_{\rm H} \int (n/n_0) 2\pi r\, dr\, dz} = \frac{G M_{\rm disk}^2}{128\pi\mu m_{\rm H} c^2 R^4} . \quad (8)$$

In Figure 1 we show the formation redshift dependence of the number density n_0, scale radius R, and the ratio $z_0(r = R)/R$ for disks of different masses. To compare with the Milky Way, we examine the results for $M_{\rm halo} = 10^{12}\ M_\odot$ and $z_f = 1$. This gives $n_0 \approx 100$ cm^{-3}, a scale length $R \approx 5$ kpc, and $z_0(r = R)/R \approx 0.002$, yielding a disk that is denser and thinner than that of the Milky Way. The discrepancy results from our choice of $m_d = 0.17$, whereas for the Milky Way the disk mass today is a reduced fraction $m_d \sim 0.05$ of the halo mass, possibly due to the effects of supernovae-driven outflows or inefficient cooling of the cosmic gas (the latter phenomenon could be important at $z \lesssim 2$ when the IGM becomes rarefied and hot but is likely to be irrelevant for galaxies which form at higher redshifts out of the much denser and cooler IGM). A value of $m_d = 0.05$ indeed yields $n(r = 2R) \approx 1$ cm^{-3} and $z_0(r = 2R)/R \approx 0.04$, more appropriate for the mean baryonic density in the solar neighborhood.

We emphasize that fragmentation of the gas into stars or quasar black holes is only possible as a result of substantial cooling of the gas well below its initial virial temperature. Since molecular hydrogen is likely to be photodissociated in the low-metallicity gas of primeval galaxies (Haiman, Rees, & Loeb 1997; Omukai & Nishi 1999), only atomic cooling is effective, and so stars and quasars are likely to form only in halos with a virial temperature $\gg 10^4$ K, where atomic cooling is effective. We therefore restrict our attention to such halos. Inside such halos, thin disks can exist for our assumed gas temperature of $\sim 10^4$ K.

We restrict our simulations to halos in the range 10^9–$10^{12}\ M_\odot$. The gas in lower mass halos is either unable to cool and form stars (due to the ease by which the only available coolant, H_2, is photodissociated) or is boiled out of the shallow gravitational potential wells of the host halos by photoionization heating of hydrogen to $\gtrsim 10^4$ K (above the virial temperature of these halos) as soon as a small number of ionizing sources form (Omukai & Nishi 1999; Nishi & Susa 1999; Barkana & Loeb 1999). If low-mass halos lose their gas quickly, then their contribution to the ionizing background can be evaluated trivially from their assumed star formation efficiency, with no need for a detailed radiative transfer calculation. The most popular cosmology at present involves a ΛCDM power spectrum of density fluctuations with $\Omega_m = 0.3$, $\Omega_\Lambda = 0.7$, $\sigma_8 = 0.9$, $h = 0.7$, and $n = 1$ (scale invariant spectrum). For this cosmology we find that halos with a dark matter mass of $10^9\ M_\odot$ are 1.4 σ fluctuations at $z = 5$ and 2.5 σ fluctuations at $z = 10$. Halos of mass $10^{12}\ M_\odot$ are 2.9 σ fluctuations at $z = 5$ and 5.3 σ fluctuations at $z = 10$.

2.2. *Illumination*

We consider two separate cases for the sources of ionizing radiation within the galactic disks: stars and quasars. Below we describe the luminosity and the spatial location of the sources in these different cases.

2.2.1. *Stars*

In Monte Carlo simulations of the transfer of star light through galaxies, the stellar sources are often represented by a smooth spatial distribution (e.g., Wood & Jones 1997; Ferrara et al. 1996, 1999; Bianchi, Ferrara, & Giovanardi 1996) rather than by individual point sources (but see recent work by Cole, Wood, & Nordsieck 1999; Wood & Reynolds 1999). In our simulations, we consider two smooth distributions for the stellar emissivity: $j_* \propto n(r, z)$ and $j_* \propto n(r, z)^2$. In the first case, we are assuming that the star formation efficiency is independent of density, while in the second case the stars are assumed to form preferentially in denser gaseous regions. Note that the second prescription reproduces the observed Schmidt law for the star formation rate of spiral galaxies as a function of the disk surface density (Kennicutt 1998).

We assume a sudden burst of (metal-poor) star formation with a Scalo (1986) stellar mass function and adopt a corresponding ionizing luminosity of $Q_*(H^0) = 10^{46} M_*/M_\odot$ s^{-1}, where M_* is the stellar mass of the galaxy (Haiman & Loeb 1997). This luminosity is consistent with detailed models of starburst galaxies (e.g., Leitherer et al. 1999). The stellar mass is defined by the fraction of gas which gets

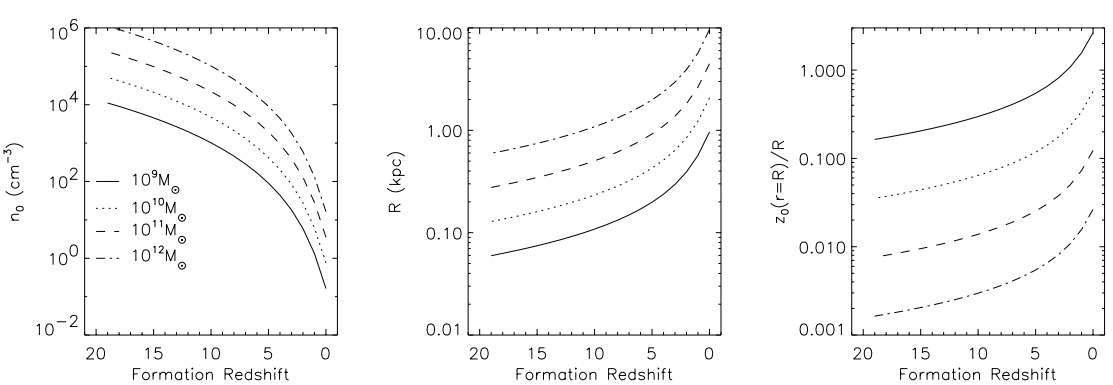

FIG. 1.—Central densities, scale lengths, and the ratio of scale height/scale length as functions of redshift, for our model of isothermal, self-gravitating disks that form within dark matter halos of various masses.

converted into stars, $M_* = f_* M_{\rm disk}$. We consider two cases (independent of formation redshift), namely, $f_* = 0.04$ and $f_* = 0.4$, with the gaseous disk being reduced in mass by the factor $1 - f_*$. The value $f_* = 0.04$ was used by Haiman & Loeb (1997) so as to reproduce the observed metallicity of $\sim 0.01\ Z_\odot$ in the IGM at $z \sim 3$ (Tytler et al. 1995; Songaila & Cowie 1996). We also consider a higher value of $f_* = 0.4$, in case $\sim 90\%$ of all the metals are retained within their host galaxies and only $\sim 10\%$ are mixed with the IGM. Since the actual IGM metallicity at $z \sim 3$ might be in the lower range of 0.1%–1% $Z_\odot$ (Songaila 1997), our assumed values for f_* and the corresponding ionizing fluxes might be considered as high. The corresponding ionization fraction of the disk is overestimated, and our derived escape fractions should therefore be regarded as upper limits.

In summary, the total ionizing luminosity for stellar sources in our simulations is related to the halo mass via

$$Q_*(\mathrm{H}^0) = 10^{46} m_d f_* \frac{M_{\rm halo}}{M_\odot}\ \mathrm{s}^{-1}\ . \tag{9}$$

Our code assumes a constant value for this ionizing luminosity and solves for the ionization structure of the disk and the consequent escape fraction in a steady state. Since the characteristic time over which a starburst would possess the ionizing luminosity in equation (9) is $\sim 3 \times 10^6$ yr for a Scalo (1986) stellar mass function (see Fig. 4 in Haiman & Loeb 1997), the star formation rate required in order to maintain a steady ionizing luminosity of this magnitude is

$$\dot{M}_* \approx \frac{f_* M_{\rm disk}}{3 \times 10^6\ \mathrm{yr}} = 23 \frac{M_\odot}{\mathrm{yr}} \left(\frac{f_*}{0.04}\right)\left(\frac{M_{\rm halo}}{10^{10}\ M_\odot}\right). \tag{10}$$

This is a rather high star formation rate, as it implies that for $f_* \sim 4\%$ the entire disk mass will be converted into stars in less than a Hubble time at $z \sim 10$. The assumed star formation rates are unreasonably high for $f_* = 40\%$ and large halo masses (e.g., $\dot{M}_* \sim 2 \times 10^4\ M_\odot\ \mathrm{yr}^{-1}$ for $M_{\rm halo} \sim 10^{12}\ M_\odot$). For this reason, one may regard our calculated escape fractions as upper limits.

In order to perform the photoionization calculation with our Monte Carlo code, we need to specify the flux-weighted mean of the opacity of neutral hydrogen for a given ionizing spectrum (see § 2.3 and the Appendix). We adopt a flux mean cross section of $\bar{\sigma} = 3.15 \times 10^{-18}\ \mathrm{cm}^2$, which is appropriate for the composite Scalo initial mass function emissivity spectrum presented in Figure 3 of Haiman & Loeb (1997).

2.2.2. *Quasars*

In the case of a quasar we assume that the ionizing radiation emanates from a point source at the center of the disk. Haiman & Loeb (1998, 1999) have demonstrated that the observed B-band and X-ray luminosity functions of high-redshift quasars at $z \gtrsim 2.2$ can be fitted by a ΛCDM model in which each dark matter halo harbors a black hole with a mass

$$M_{\rm BH} = m_{\rm bh} M_{\rm halo}\ , \tag{11}$$

which shines at the Eddington luminosity, $L_{\rm Edd} = 1.4 \times 10^{38} (M_{\rm BH}/M_\odot)$ ergs s^{-1}, for a period of $\sim 10^6$ yr when the halo forms. The required value of $m_{\rm bh} \approx 6 \times 10^{-4}$ is consistent with the inferred black hole masses in local galaxies (Magorrian et al. 1998). We will adopt this prescription in deriving the quasar luminosity within a halo of a given mass. As there is a large scatter around the mean in the observed distribution of the black hole/bulge mass ratio, we also consider lower values in the range $6 \times 10^{-7} < m_{\rm bh} < 6 \times 10^{-4}$ for a $10^{10}\ M_\odot$ halo (see § 3.2).

The ionizing component of quasar spectra is not well determined empirically; we use the calibration of Laor & Draine (1993) and relate the ionizing luminosity to the total bolometric luminosity by $Q_{\rm QSO}(\mathrm{H}^0) = 6.6 \times 10^9 (L_{\rm Edd}/\mathrm{ergs\ s}^{-1})\ \mathrm{s}^{-1}$. Hence, the ionizing luminosity of a quasar in our models is related to its host halo mass through

$$Q_{\rm QSO}(\mathrm{H}^0) = 9.24 \times 10^{47} m_{\rm bh} \frac{M_{\rm halo}}{M_\odot}\ \mathrm{s}^{-1}\ . \tag{12}$$

We consistently adopt a flux-weighted mean of the opacity for the characteristic quasar spectrum of $\bar{\sigma} = 2.05 \times 10^{-18}$ cm^2 (Laor & Draine 1993).

2.3. *Radiation Transfer*

In our simulations we employ a three-dimensional Monte Carlo radiation transfer code (Wood & Reynolds 1999) that has been modified to include photoionization. Our photoionization code is similar to that of Och et al. (1998) but somewhat simplified in that we only treat the photoionization of hydrogen at a constant temperature. However, as our simulations are run on a three-dimensional grid we are able to investigate complex geometries which are relevant to the present study. We track the propagation of ionizing photons from the source as they are absorbed and reemitted as diffuse ionizing photons or as nonionizing photons (in which case they are subsequently ignored). In each computational cell the contributions of each ionizing photon to the mean intensity are tallied, so that we may determine the ionization fraction throughout our grid. We iterate on this procedure until the ionization fractions converge. We keep track of the number of ionizing photons that exit our grid either directly from the source or after multiple absorption and reemission as diffuse ionizing photons, thus determining the escape fraction of ionizing radiation. Note that we consider escaping ionizing photons to be either direct photons from the source or diffuse photons. As with most models of the escape of ionizing photons, we have not considered the detailed effects of the ionizing spectrum and work with a total ionizing luminosity (e.g., Miller & Cox 1993; Dove & Shull 1994; Dove et al. 2000; Razoumov & Scott 1999). Where our work differs from "Strömgren volume" analyses is that we calculate the ionization fraction throughout our grid and track diffuse (absorbed and reemitted) ionizing photons also. A more detailed description of our code and its comparison with other photoionization calculations are presented in the Appendix.

Our code is time independent and does not consider any time evolution of the ionizing spectrum in the calculation of the escape fraction. Stellar evolution models imply that the ionizing luminosity remains fairly constant for $\lesssim 10^7$ yr (a typical main-sequence lifetime of an O star) and decreases subsequently (Haiman & Loeb 1997; Leitherer et al. 1999). In recent modeling of the Milky Way, Dove et al. (2000) showed that including the time dependence (and also the effects of dynamical supershells) results in a decrease of the escape fractions compared to their static calculations (Dove & Shull 1994). Therefore, we will tend to overestimate the escape fraction since we ignore the time decay of the ionizing luminosity, and our results will provide upper limits

for the escape of stellar ionizing radiation from smooth galactic disks. For quasars, Haiman & Loeb (1998) found that the observed quasar luminosity functions are best fit with a quasar lifetime of $\sim 10^6$ yr. As for the stellar case, our static quasar models yield upper limits on the escape fraction. However, since the maximum ionizing luminosity of quasars is higher by $\gtrsim 2$ orders of magnitude than that of stars and involves harder photons, and since it all originates from a single point, the propagation of the ionization front is expected to be much faster for quasars, and so the steady state assumption should, in fact, be more adequate in their case.

For both stars and quasars, we ignore at first the effects of energetic outflows on the galactic disk. Outflows could clear away material and raise the calculated escape fractions. We will incorporate this dilution effect by artificially reducing the absorbing gas mass in the disk in some of the numerical runs.

3. RESULTS

3.1. *Stars*

We calculated the escape fraction of stellar ionizing radiation by simulating the disk out to a radius of $3R(z_f)$ and using a smooth emissivity profile in it. As the disk density increases with redshift, the recombination rate increases and the ionizing luminosity of the galaxy results in a lower ionization fraction, leading to a decrease in the escape fraction with increasing redshift.

Figure 2 shows the escape fraction as a function of formation redshift for various halo masses, assuming $f_* = 4\%$ and emissivities $\propto n^2$ (Fig. 2*a*) and $\propto n$ (Fig. 2*b*). In these models the largest escape fractions occur for low-mass disks, but the escape fractions are $f_{\rm esc} < 0.1\%$ at $z_f > 5$. When the emissivity scales as $\propto n^2$, the sources are embedded more deeply within the disk, leaving a larger column of hydrogen to be ionized and thus leading to smaller escape fractions than in the case where the emissivity is $\propto n$.

The efficiency of converting baryons into stars is a free parameter, f_*, in our models. In Figure 3 we show escape fractions for the much larger efficiency, $f_* = 40\%$. As expected, the escape fractions are larger than the corresponding values shown in Figure 2 due to the increased ionizing luminosity (see eq. [9]) and the reduced mass of the gaseous disk in the simulations. However, the escape fractions are very small at high redshifts, certainly much smaller than the value of $f_{\rm esc} \approx 50\%$ adopted by Madau (1999) as necessary for stellar sources to keep the intergalactic medium ionized at $z \sim 5$.

In Figure 4 we show results for a simulation in which $f_* = 4\%$ but with an order-of-magnitude reduction in the density of the smooth gaseous disk, $n_0 \rightarrow n_0/10$. Since we keep the scale height of the smooth gas unchanged, this is equivalent to lowering the mass of the absorbing gas in the disk by a factor of 10 and may result from the incorporation of gas into highly dense and compact clumps (see § 4) or expulsion of gas by stellar winds and supernovae. The baryonic mass fraction in local disk galaxies, such as the Milky Way, could have been influenced by outflows, as it is a few times lower than the standard cosmic baryonic fraction of $m_d = 0.17$ (see Fig. 5). The role of feedback from outflows is expected to be more pronounced at high redshifts, where the characteristic potential well of galaxies is shallower. Note, however, that under these conditions the overall star formation efficiency is expected to be reduced. Nevertheless, in our calculation we left the stellar luminosity unchanged and only reduced the mass of the smoothly distributed gas; under these circumstances, $f_* = 4\%$ corresponds to the stars having 40% of the smooth gaseous disk mass. This calculation was intended to simulate the most favorable conditions for the escape of ionizing radiation from high-redshift disks. Figure 4 illustrates that although the resulting escape fractions for this extreme case are larger than the corresponding results in Figure 2, they are still negligible for halo masses $M_{\rm halo} > 10^{10}\ M_\odot$ at $z_f > 10$. It should be further noted that these low escape fractions were calculated for the steady ionization state of the disk implied by the rather high star formation rates in equation (10). We also examined the case of gas removal from the disk due to outflows, resulting in an increased disk scale height. Escape

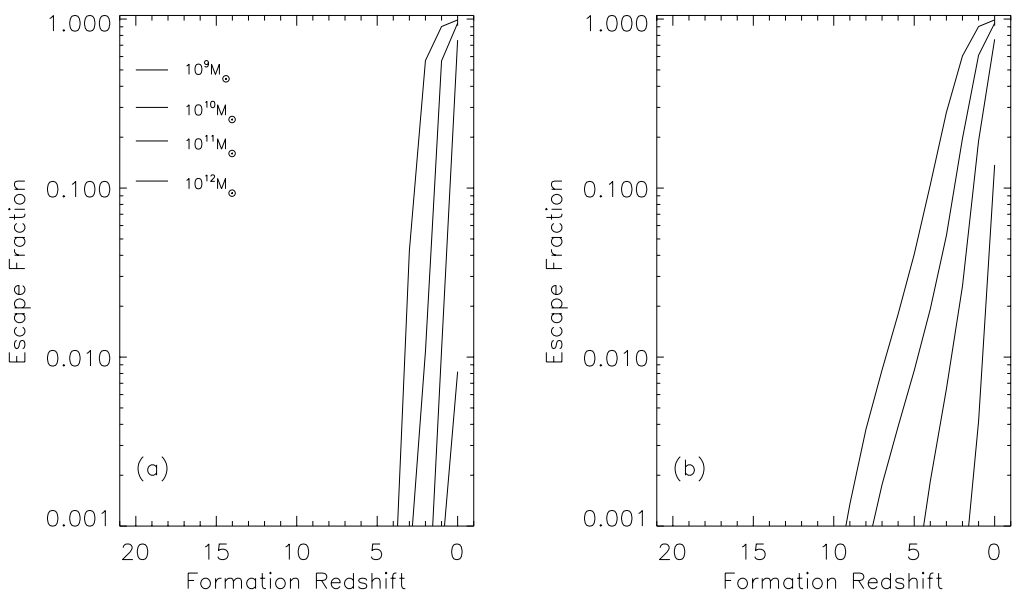

FIG. 2.—Stellar escape fractions for smooth density disks within dark matter halos of different masses, assuming $f_* = 4\%$. (*a*) Ionizing emissivity distributed $\propto n^2$. (*b*) Ionizing emissivity distributed $\propto n$.

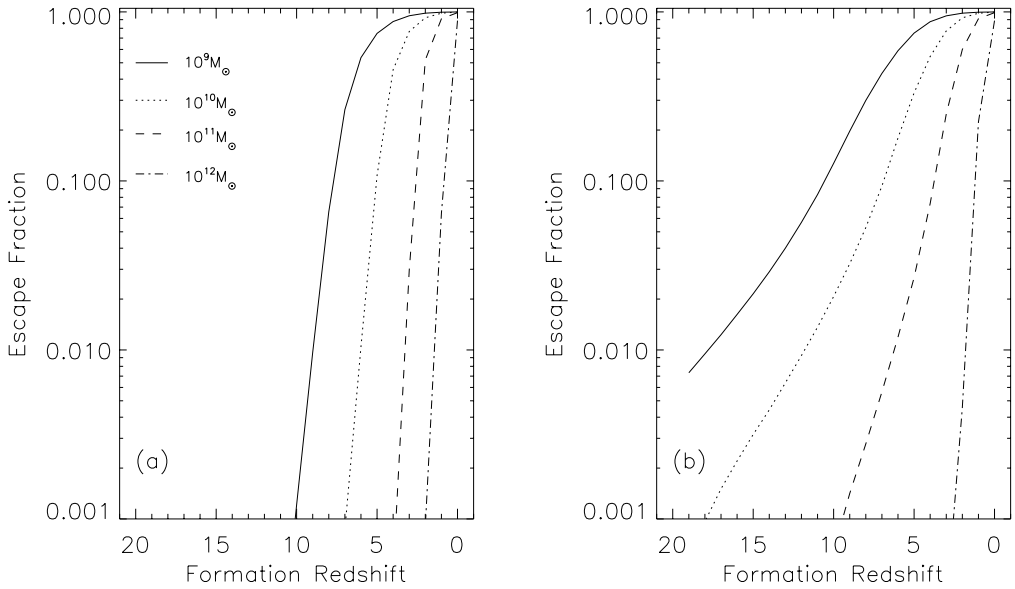

FIG. 3.—Same as in Fig. 2 but for $f_* = 40\%$

fractions for reducing the central density, n_0, by a factor of 10 (or correspondingly the disk mass by a factor of 3 in this case) yield results very similar to those in Figure 4.

In order to investigate the effects on the escape fractions of a lower disk mass than our assumed $m_d = 0.17$, we have performed a simulation for a $10^{10}\ M_\odot$ halo assuming $f_* = 4\%$ and $j_* \propto n$ but with $m_d = 0.02$. The results are shown in Figure 5. The lower disk mass yields a lower ionizing luminosity (eq. [9]) and a lower gas density (eq. [8]). The overall result of this is an increase in the escape fraction, albeit for galaxies of intrinsically lower luminosity.

3.2. *Quasars*

Being a point source of ionizing radiation, a quasar is expected to create an ionized region around the center of the galactic disk. The disk geometry presents a higher opacity to the quasar's ionizing photons along the disk midplane than it does perpendicular to it. If the quasar luminosity is sufficiently high, it creates a vertically extended photoionized region of low opacity through which ionizing photons may escape. We have therefore restricted our simulations of quasar sources to the innermost region of the disk and performed the radiation transfer within a cube of size $40 z_0 (r = 0)$ on a side.

Figure 6 presents the escape fraction as a function of formation redshift for various halo masses. The escape fractions are typically in the range of 20%–80% over a wide range of formation redshifts and halo masses. They decrease as the disks get denser with increasing formation redshift but are always significantly larger than for the stellar case. In all our simulations, the vertical escape routes are created by the ionizing luminosity of the quasar without consider-

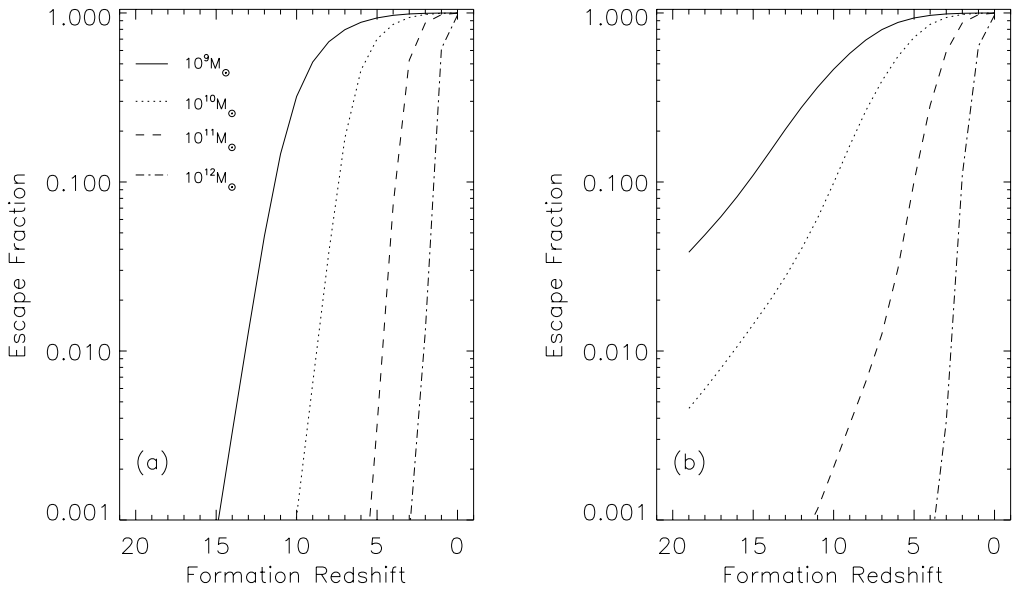

FIG. 4.—Same as in Fig. 2 but with an order-of-magnitude reduction in the density of the smooth gaseous disk, or $n_0 \rightarrow n_0/10$

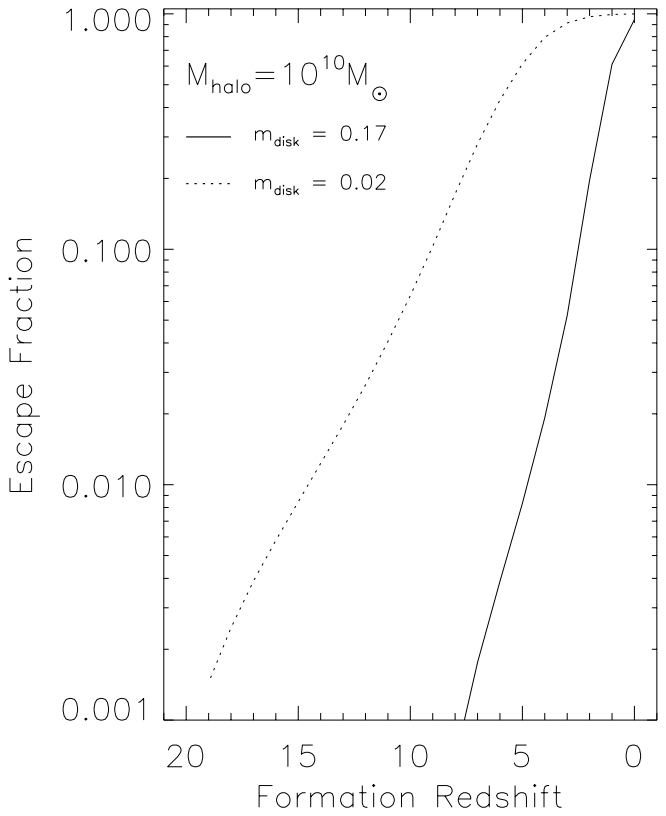

FIG. 5.—Escape fractions of stellar ionizing photons from a smooth disk within a 10^{10} $M_\odot$ halo. The curves represent the cases when the ratio of disk mass to halo mass is $m_d = 0.17$ and $m_d = 0.02$.

ing any additional dynamical clearing of the gas by outflows (e.g., a jet or a wind) from the quasar. Such dynamical action could open up low-density escape routes for the ionizing photons, thereby increasing the already high escape fraction. In Figure 6*b* we show escape fractions assuming the gaseous disk has a density smaller by a factor of 10 than considered in Figure 6*a* ($n_0 \rightarrow n_0/10$). As expected, the escape fractions are very high in this case.

Our derivation of high escape fractions for quasars is consistent with the lack of significant absorption beyond the Lyman limit at the host galaxy redshift in observed quasar spectra (see, e.g., review by Koratkar & Blaes 1999).

We have also simulated lower luminosity quasars ionizing a disk within a 10^{10} $M_\odot$ halo. Figure 7 shows the escape fractions for black hole masses in the range $6 \times 10^{-7} < m_{bh} < 6 \times 10^{-4}$. Since the ionizing luminosity is proportional to the black hole mass (see eqs. [11] and [12]), the escape fraction decreases for low-luminosity quasars. For very low luminosity quasars f_{esc} diminishes because the Strömgren sphere created by the quasar is smaller than the scale height of the disk and all ionizing photons are trapped. In these cases, the emergence of hydrodynamic outflows or jets from the quasar accretion flow could be important in opening escape channels for the ionizing radiation.

3.3. *Angular Distribution of Escaping Ionizing Flux*

In addition to the ionization structure and escape fraction, our code also provides the angular distribution of the escaping ionizing flux. In Figure 8 we show this angular distribution for stellar sources ($f_* = 4\%$) or a central quasar within a halo of mass $M_{halo} = 10^{10}$ $M_\odot$ at $z_f = 8$. The escape fraction for the stellar case is $f_{esc} = 6\%$ and for the quasar $f_{esc} = 60\%$. Since the system is axisymmetric in both cases, we show the normalized flux of ionizing photons as a function of cos *i*, where *i* is the disk inclination angle. The flux is normalized to unity for a face-on viewing of the disk. The figure clearly illustrates the asymmetry of the emerging ionizing radiation field due to the dense disk, as photons escape preferentially along the paths of lower optical depth. For the quasar case the pole-to-equator flux ratio is more extreme since the central source opens up a low-opacity ionized chimney and is unable to ionize the disk to a large

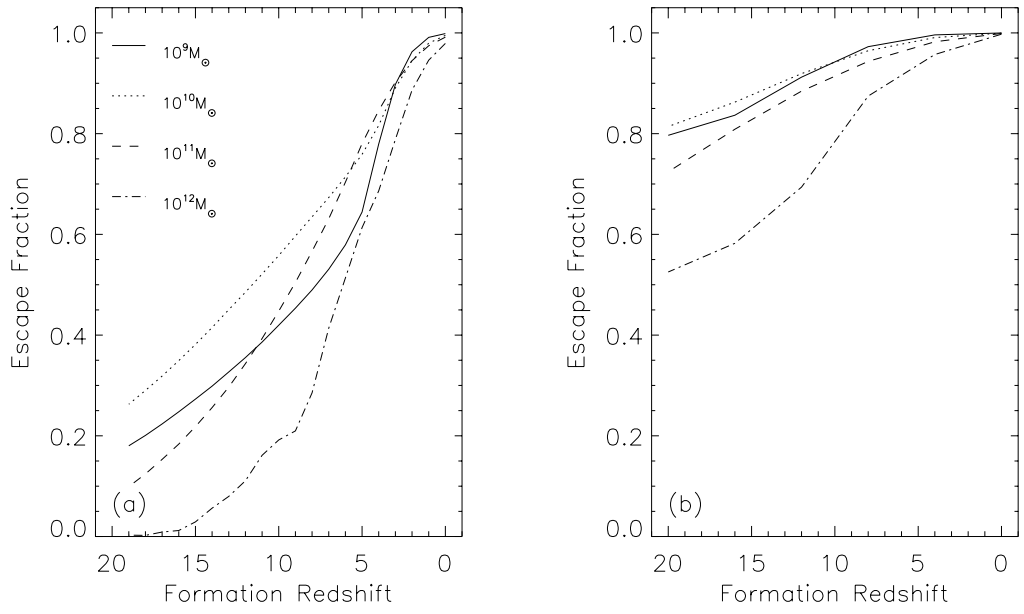

FIG. 6.—Escape fractions for ionization of galactic disks within dark matter halos of different masses by a central quasar. (*a*) Disk number density given by eq. (8). (*b*) Diluted disk mass, $n_0 \rightarrow n_0/10$.

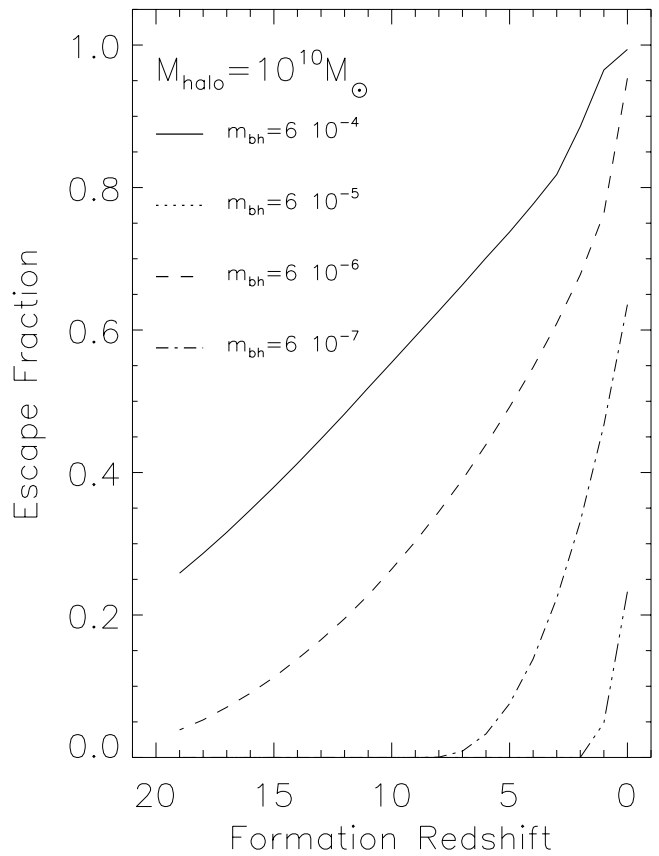

FIG. 7.—Escape fractions of quasar ionizing photons from a smooth disk within a $10^{10}\ M_\odot$ halo. The curves represent the cases when the ratio of black hole mass to halo mass is in the range $6 \times 10^{-7} < m_{bh} < 6 \times 10^{-4}$. The quasar luminosity is assumed to be proportional to the black hole mass, so the escape fractions are smaller for lower mass black holes.

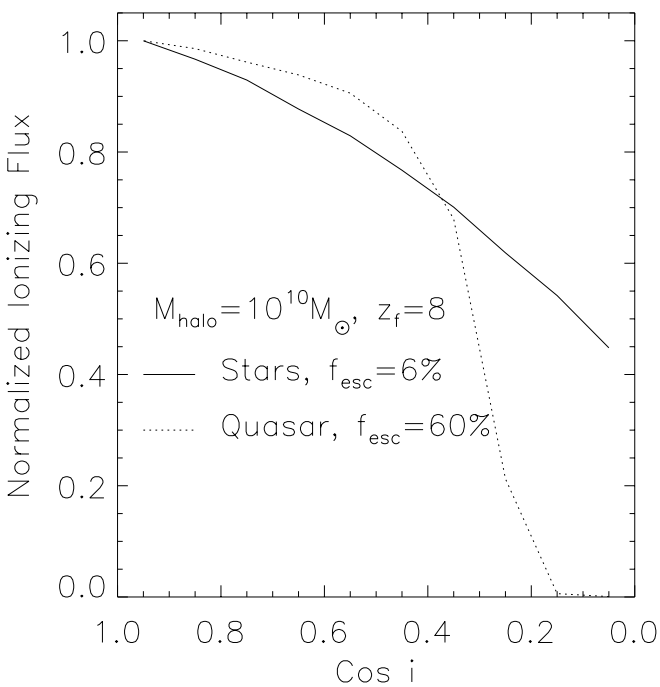

FIG. 8.—Angular distribution of the escaping ionizing flux from a quasar or stars within a dark matter halo of $M_{halo} = 10^{10}\ M_\odot$ at $z_f = 8$. The flux is arbitrarily normalized to unity for a disk inclination angle $i = 0°$.

distance in the midplane. For stars the emission is distributed throughout the disk resulting in a more moderate pole-to-equator flux variation. The cosmological H II regions formed by both types of sources in the surrounding IGM will show neutral shadow regions aligned with the disk midplane.

4. EFFECTS OF CLUMPING ON THE ESCAPE OF IONIZING RADIATION FROM STARS

In § 3.1 we calculated the escape fraction, f_{esc}, for stellar sources, assuming that the ionizing sources and absorbing galactic gas were smoothly distributed according to the formulae presented in § 2.2. In this section we present results of simulations where either the gas, the sources, or both have a clumpy distribution within the galactic disks. Several recent papers have studied the dust scattering of radiation in a two-phase medium, with emphasis on the penetration and escape of nonionizing stellar radiation from clumpy environments (Boissé 1990; Witt & Gordon 1996, 2000; Bianchi et al. 2000; Haiman & Spaans 1999). Dove et al. (2000) investigated the escape of ionizing photons from the Milky Way disk where inhomogeneities in the interstellar medium were modeled as either spheres or cylindrical disks. In all of these studies, clumping allowed photons to penetrate to greater depths than in a smooth medium, and the escape of radiation was enhanced relative to the case where the same gas mass was distributed smoothly.

In evaluating the escape of ionizing radiation from clumpy environments, we adopt the two-phase prescription from Witt & Gordon (1996). The two-phase medium has two parameters, namely, the volume filling factor of dense clumps, ff, and the density contrast between the clump and interclump medium, C. We transform our smooth density distribution (eqs. [6], [7], and [8]) into a clumpy one by looping through our three-dimensional grid and applying the following algorithm in each grid cell:

$$n_{clumpy} = \begin{cases} n_{smooth}/[ff + (1-ff)/C] & \text{if } \xi < ff\ , \\ n_{smooth}/[ff(C-1)+1] & \text{otherwise}\ , \end{cases} \quad (13)$$

where ξ is a uniform random deviate in the range (0, 1). This algorithm assures that *on average* the total disk mass is the same for the clumpy and smooth models and that the ensemble average of the clumpy distribution follows the same spatial profile as the smooth gas does. In this approach the smallest clump is a single cell in our density grid. Our resolution is set by the size of our density grid (100^3 cells), so that each cell is a cube of size $3R/50$, where R is the radial scale length of the disk. For simplicity, we consider a two-phase medium for which the interclump medium has a zero density. Such a medium is described by a single parameter only, ff. In our simulations we approximate this extreme case by adopting a very large density contrast $C = 10^6$. Slices through the resulting density distribution for various clump filling factors are shown in Figure 9. We have also applied the above algorithm to generate a clumpy emissivity distribution, which could result, for example, from clusters of young stars.

In Figure 10 we show results of clumpy simulations for the case of a $10^{10}\ M_\odot$ halo at $z_f = 10$, where $m_d = 0.17$, $f_* = 4\%$, and $j_* \propto n$. In our smooth simulations this yields $f_{esc} < 10^{-3}$. The figure shows the results of three different clumpy simulations. The first simulation assumes a smooth distribution for the gas and a clumpy distribution for the

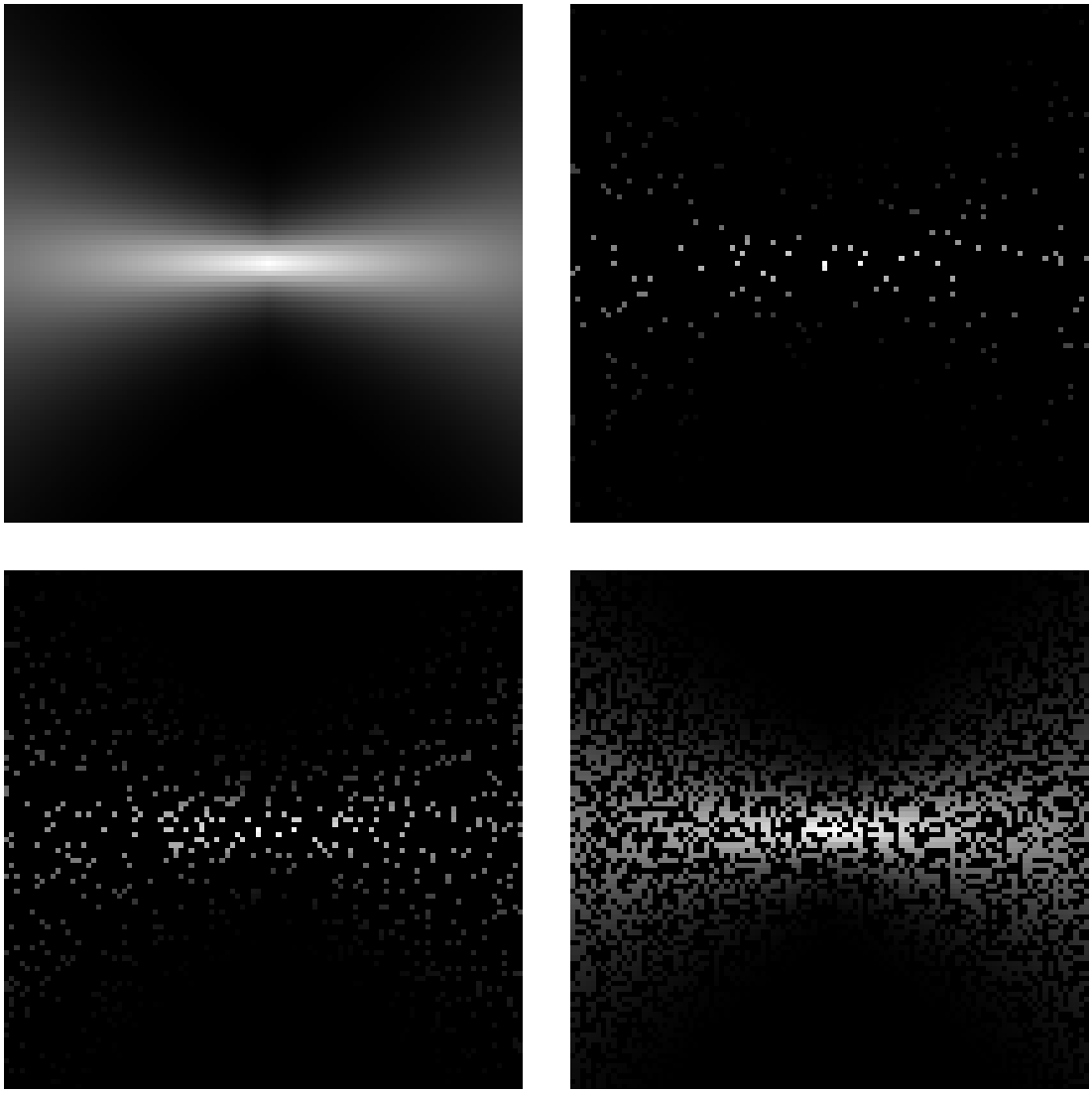

FIG. 9.—Slices through a disk formed within a $10^{10}\ M_{\odot}$ halo at $z_f = 10$. The panels show the smooth case (*upper left panel*) and three clumpy cases. The different clumpy models are for various volume filling factors of dense clumps: $ff = 3\%$ (*upper right panel*); $ff = 10\%$ (*lower left panel*); $ff = 50\%$ (*lower right panel*). All panels show the fourth root of the number density $n^{1/4}$.

emissivity, while the second examines a clumpy gas and a smooth emissivity distribution. In the third simulation both the emissivity and the gas density are clumped, but they are not spatially correlated (i.e., we generated the clumpy density and emissivity with the above algorithm but from different random number sequences).

For the first simulation, ff is defined to be the filling factor of the clumpy emissivity. We find that $f_{\rm esc} > 1\%$ is attained for $ff < 0.05$. For these very low values of ff, the emissivity is concentrated into less than 5% of the galactic volume. Within these compact concentrations there is a higher flux of ionizing photons per hydrogen atom compared to the smooth simulations. Each high-emissivity cell can now generate a bigger Strömgren volume and, depending on its location within the galactic disk, can open up an H II escape channel and yield a larger $f_{\rm esc}$ than the smooth simulation does. As the emissivity filling factor approaches unity, we retrieve the very small $f_{\rm esc}$ characteristic of the smooth case.

The escape fractions are larger when the interstellar medium is clumped. We find that with the above prescription for the random clumping the results are insensitive to whether the emissivity is smooth or clumped. (However, when the clumpy emissivity and density are correlated, i.e., emission arises only within the dense clumps, we find that the escape fraction is negligible since the emission within the dense clumps is unable to ionize the clumps and escape.) When the clump filling factor is small, there are lines of sight from either the smooth or clumpy emissivity that do not encounter dense gas and the ionizing photons are free to directly exit the galactic disk. The escape fraction approaches unity for very small clump filling factors. Such small filling factors represent the unphysical situations of all the galactic mass residing in a few dense and highly compact clumps. However, we do find $f_{\rm esc}$ can exceed several percent for $ff \approx 20\%$ which is comparable to the filling factors of H I (Bregman, Kelson, & Ashe 1993) and H II (Reynolds et al. 1995) in the Milky Way. While the two-phase density distribution we have adopted does not fully describe the hierarchical structures observed in galactic disks, it does provide an estimate of the porosity levels

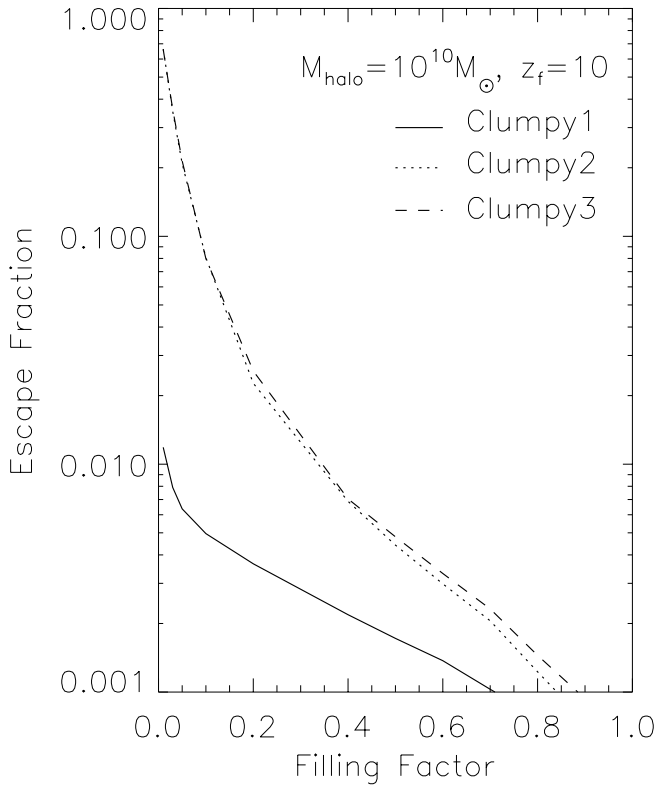

FIG. 10.—Escape fractions of stellar ionizing photons from a disk within a 10^{10} $M_\odot$ halo formed at $z_f = 10$. The curves show different clumpy models. The volume filling factor refers to either the ionizing emissivity, the clumps, or both, depending on the case. Clumpy1: clumpy emissivity, smooth interstellar medium (ISM); clumpy2: smooth emissivity, clumpy ISM; clumpy3: uncorrelated clumpy emissivity and clumpy ISM.

and clump filling factors required to allow significant escape fractions from high-redshift galaxies.

5. DISCUSSION

We have calculated the escape fraction of ionizing photons as a function of formation redshift, z_f, for disk galaxies of various masses. In our canonical model, the disk mass within a given dark matter halo was assumed to be the cosmic baryonic mass fraction, since the initial cooling of the virialized gas with a temperature $T \gtrsim 10^4$ K is expected to be very rapid compared to a Hubble time at the high redshifts of interest (see relevant cooling rates in Binney & Tremaine 1987). We find that for smooth disks the escape fraction for bright quasars is in excess of $\sim 30\%$ for most galaxies at $z_f > 10$, whereas stellar sources are unable to ionize their host galaxies, yielding much smaller escape fractions. In our smooth disk models, stellar escape fractions in excess of a percent are never achieved beyond $z_f = 10$ (see Fig. 2) unless the conversion efficiency of baryons into stars, f_*, is large (Fig. 3), requiring unreasonably high star formation rates (see eq. [10]). Even for the most extreme cases, we find that disks which form within rarer dark matter halos more massive than 10^{10} $M_\odot$ have negligible escape fractions at $z_f \gtrsim 10$.

Clumping or expulsion of gas from the disks would tend to leave a diluted interstellar medium and allow for larger escape fractions. We have investigated the effect of gas expulsion by considering a smooth gaseous disk in which the density is an order of magnitude lower than implied by the cosmic baryonic fraction (see Figs. 4 and 5). In this case we find that the escape fractions are considerably increased, but again only disks within low-mass halos ($M_{\rm halo} \lesssim 10^{10}$ $M_\odot$) exhibit escape fractions in excess of several percent at $z_f \gtrsim 10$. Note that this case requires an extreme star formation rate even with $f_* = 4\%$, since 40% of the smooth gas mass is already incorporated into stars. If the depletion of the smooth gas is due to outflows, then these flows would be effective at increasing the escape fraction only if they clear out the absorbing gas from the disk in less than a few million years, the characteristic timescale over which the ionizing radiation is emitted by massive stars. In this case, the overall star formation efficiency is expected to be lower than we assumed due to the rapid depletion of the galactic gas reservoir (and so the total contribution of the host galaxy to the ionizing background would be low). We have also investigated the escape fractions from clumpy disks with a two-phase density distribution and find that escape fractions larger than a few percent can be achieved if the interclump regions (which were assumed to be devoid of absorbing material) occupy $\gtrsim 80\%$ of the disk volume.

In all our simulations we have calculated escape fractions for the asymptotic steady ionization state of the disk. Unless the star formation rates maintain the high values implied by equation (10) over several generations of massive stars, our simulations overestimate the escape fractions since they do not include the lower ionization state of the surrounding gas due to the lower ionizing luminosity at both early and late times. Considering the Milky Way, Dove et al. (2000) have shown that including the effects of a finite source lifetime and radiation transfer through supershells created by stellar winds and supernovae will *decrease* the escape fractions compared to the smooth, static cases we have considered. We expect this effect to be less important for quasars than it is for stars; due to their much higher brightness, quasars reach steady ionization conditions on a timescale much shorter than their expected lifetime (which is $\gtrsim 10^6$ yr).

Our discussion focused on isothermal ($T = 10^4$ K) disks that form within dark matter halos with masses $M_{\rm halo} \geq 10^9$ $M_\odot$. Lower mass halos yield disk scale heights that are not smaller than their scale radii (see Fig. 1), since their virial temperature is lower than our assumed gas temperature of 10^4 K. The virialized gas in such halos is unable to cool via atomic transitions and might fragment into stars only if molecular hydrogen forms efficiently in it (Haiman, Abel, & Rees 2000). However, the star formation process in such systems is expected to be self-destructive and to limit f_* to low values. If only a small fraction of the gas converts into massive stars, then molecular hydrogen would be photodissociated (Omukai & Nishi 1999). More importantly, any substantial photoionization of the gas in these systems (which is required in order to allow for a considerable escape fraction) would heat the gas to a temperature $\gtrsim 10^4$ K and boil it out of the gravitational potential well of the host galaxy, thus suppressing additional star formation. Winds from a small number of stars or from a single supernova could produce the same effect. It is, of course, possible that by the time the gas is removed from these systems they would have already formed stars that contribute to the ionizing background. However, the star formation efficiency under these circumstances is expected to be significantly lower than in higher mass galaxies.

Our derived escape fractions should be regarded as upper limits since more absorption is likely to be added by neutral

gas in the vicinity of the galaxies, due to infalling material, gas in galaxy groups, or gas in nearby intergalactic sheets and filaments. The surrounding gas density is expected to decline rapidly with distance away from a galactic source (roughly as $\propto 1/r^{2.2}$ in self-similar infall models; Bertschinger 1985) and so have its strongest absorption effect close to the source. Large-scale numerical simulations of reionization (e.g., Gnedin 2000) cannot resolve the small scales of interest due to dynamic range limitations and are forced to adopt ad hoc prescriptions for the escape fraction from galaxies. A natural extension of the radiation transfer calculation presented in this work would be to embed a galactic source inside its likely intergalactic environment based on high-resolution small-scale hydrodynamic simulations and to find the fraction of ionizing photons which would escape into the more distant intergalactic space.

Our calculations can be tested by spectroscopic observations of high-redshift galaxies, such as the Lyman break population at $z \sim 3$–5 (Steidel et al. 1999). While a direct detection of flux beyond the Lyman break might prove difficult, infrared observations of the Hα emission from the halos of these galaxies might be used to constrain the escape fraction of their ionizing luminosities.

The major implication of this work is that ionizing radiation from stars in high-redshift disk galaxies is expected to be trapped by their surrounding high-density interstellar medium unless outflows or fragmentation dilutes this gas by more than an order of magnitude. If most of the gas remains in the smooth disk during the lifetime of the massive stars ($\lesssim 10^7$ yr), then stellar sources are unable to contribute significantly to the intergalactic ionizing background at redshifts $z \gtrsim 6$, and only miniquasars are capable of reionizing the universe then. If miniquasars are not sufficiently abundant or have very low luminosities at these redshifts (see Fig. 7), then reionization must have occurred late, close to the horizon of current observations at $z \sim 6$–7.

K. W. acknowledges support from NASA's Long Term Space Astrophysics Research Program (NAG 5-6039) and thanks John Mathis, Jon Bjorkman, George Rybicki, and Barbara Whitney for discussions related to photoionization within the Monte Carlo radiation transfer code. A. L. was supported in part by NASA grants NAG 5-7039 and NAG 5-7768. We thank Rennan Barkana, Benedetta Ciardi, Andrea Ferrara, Marco Spaans, and Linda Sparke for discussions and suggestions on this work.

APPENDIX

MONTE CARLO PHOTOIONIZATION

Our three-dimensional Monte Carlo radiation transfer code (Wood & Reynolds 1999) has been modified to include photoionization balance in a scheme close to that of Och et al. (1998). In this Appendix we describe the simplifications that we have adopted and show comparisons of our code with other calculations.

We assume that all ionizing photons encounter an average opacity (cross section) on their random walk through our grid. The opacity in each cell is given by $n_{\rm H^0}\,\bar{\sigma}$, where $n_{\rm H^0}$ is the number density of neutral hydrogen in the cell and $\bar{\sigma}$ is the average cross section. The optical depth along a path length l through the cell is then $\tau = n_{\rm H^0}\,\bar{\sigma} l$. We use two different cross sections depending on whether the photons are directly emitted by the source or have been absorbed and reemitted as diffuse ionizing photons. The cross section we use for source photons is averaged over the flux, $\bar{\sigma} = \int_{\nu_0}^{\infty} F\sigma\,d\nu / \int F\,d\nu$, where F is the source ionizing spectrum, ν_0 is the frequency at the Lyman edge, and σ is the absorption cross section of hydrogen. The diffuse ionizing spectrum is strongly peaked at energies just above 13.6 eV, and so we set the cross section for the random walks of diffuse photons to be the hydrogen cross section at energies just above 13.6 eV, $\bar{\sigma} = 6.2 \times 10^{-18}$ cm^2. This is the main simplification we have made over the work of Och et al. (1998): we are essentially considering only two frequencies in the radiation transfer.

The simulation starts with an assumed ionization fraction throughout the grid, and then source photons are emitted isotropically and the cross section is set to its flux-averaged value. Random optical depths are chosen from $\tau = -\ln \xi$, where ξ is a random number in the range $0 < \xi < 1$. The photons are tracked along their propagation direction until they reach an interaction point at a distance s from their emission (or reemission) point, where s is determined from $\tau = \int_0^s n_{\rm H^0}\,\bar{\sigma}\,dl$. At the interaction points the photons are absorbed and reemitted as either line photons with energies $h\nu < 13.6$ eV or as diffuse ionizing photons with $h\nu > 13.6$ eV. The probability of a photon being reemitted as an ionizing photon is the ratio of the energy in the diffuse ionizing spectrum to the total energy (see eq. [16] and the accompanying discussion in Och et al. 1998). In our simulations we use the following simplified form for this probability:

$$P = \frac{\alpha_1}{\alpha_A} = 1 - \frac{\alpha_B}{\alpha_A}\,, \tag{14}$$

where α_1 is the recombination coefficient to the ground state of hydrogen (which gives the diffuse ionizing spectrum), α_B is the recombination coefficient to the excited levels, and α_A is the recombination coefficient to all levels, including the ground state. In our simulations we adopt recombination coefficients appropriate for a gas at 10^4 K (Osterbrock 1989): $\alpha_A = 4.18 \times 10^{-13}$ cm^3 s^{-1}, $\alpha_B = 2.59 \times 10^{-13}$ cm^3 s^{-1}, and thus $P = 0.38$. An absorbed photon is reemitted isotropically from its absorption point as a diffuse ionizing photon if $\xi < P$. If $\xi > P$, then the photon will be reemitted as a nonionizing photon, in which case we ignore the opacity it encounters and remove it from the simulation.

As the photons are tracked on their random walks, we calculate their contribution to the mean intensity in each cell, using the path length formula from Lucy (1999, his eq. (13]),

$$J = \frac{E}{4\pi \Delta t V} \sum l\,, \tag{15}$$

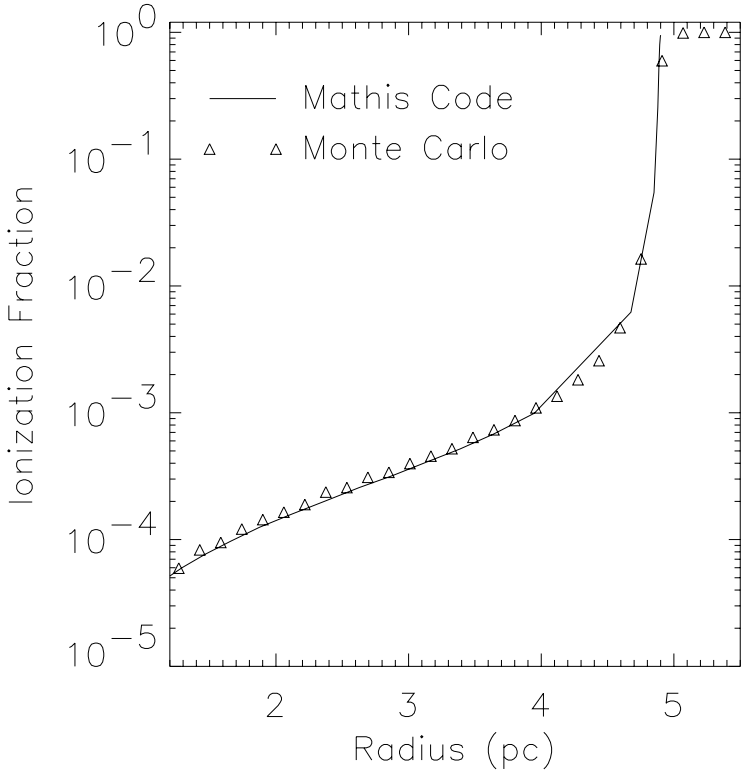

FIG. 11.—Comparison of Monte Carlo photoionization with the code of Mathis (1985). Central source of ionizing luminosity $Q(H^0) = 4.26 \times 10^{49}$ s^{-1} ionizes a region of constant number density $n_H = 100$ cm^{-3}.

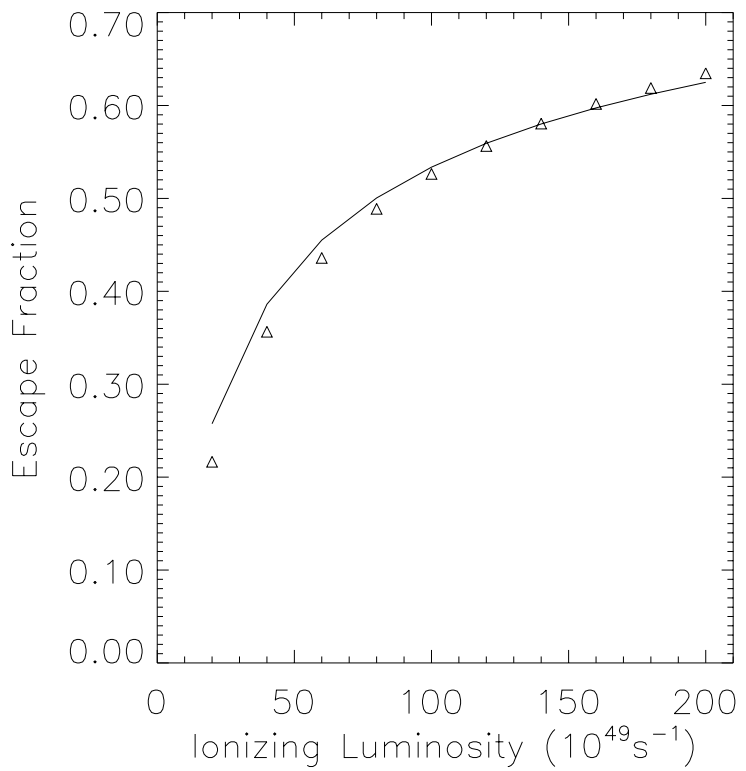

FIG. 12.—Comparison of escape fractions calculated with Monte Carlo photoionization code and the Strömgren volume approach of Dove & Shull (1994). Escape fractions are calculated for sources of different ionizing luminosity that are embedded within a three-component "Dickey-Lockman" disk. Solid curve is the analytic results from Dove & Shull (1994); triangles are Monte Carlo photoionization calculations.

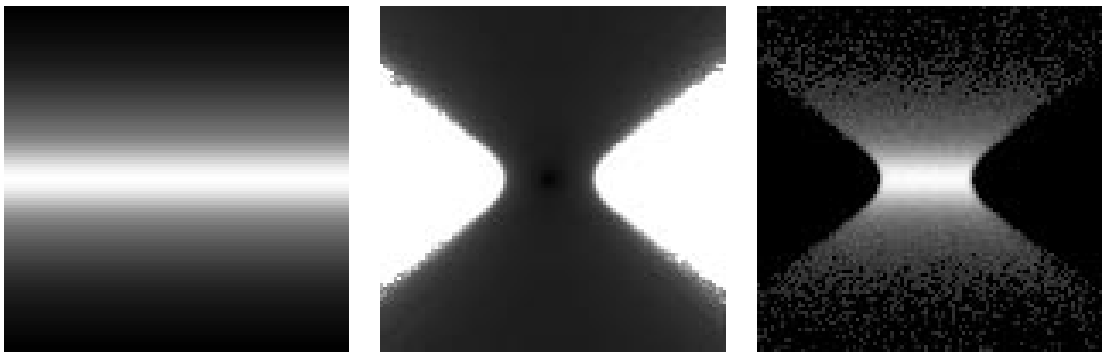

FIG. 13.—Slices through our Monte Carlo photoionization model for the $Q = 2 \times 10^{50}$ s^{-1} simulation of Fig. 12. Left panel shows the total density, middle panel illustrates the ionization fraction (white is neutral), and the right panel shows locations of absorbed photons. The nonzero H I opacity within the Strömgren volume traps some ionizing photons and explains why our escape fractions are slightly smaller than those of Dove & Shull (1994).

where the total ionizing luminosity is split up into N equal energy packets (Monte Carlo "photons") of luminosity $E/\Delta t = hvQ(\mathrm{H}^0)/N$, l is the path length the photon traverses in each cell, and V is the volume of a cell in our grid. In the photoionization equilibrium equation

$$n_{\mathrm{H}^0} \int_{\nu_0}^{\infty} \frac{4\pi J_\nu}{h\nu} \sigma_\nu \, d\nu = \alpha_A n_e n_p \, , \tag{16}$$

we need the integral of $4\pi J_\nu \sigma_\nu / h\nu$ over all ionizing frequencies. (Here n_e and n_p are the number densities of free electrons and protons.) As we are effectively only considering the cross section at two frequencies, a counter is kept for each cell that approximates the integral as

$$\int_{\nu_0}^{\infty} \frac{4\pi J_\nu}{h\nu} \sigma_\nu \, d\nu = \frac{Q(\mathrm{H}^0)}{N} \frac{\sum l}{V} \bar{\sigma} \, , \tag{17}$$

where $\bar{\sigma}$ is the mean cross section seen by either the source photons or the diffuse photons.

All photons are tracked and their contributions to the mean intensity tallied in each cell until they exit the grid either through multiple absorption and reemission as diffuse ionizing photons or as nonionizing photons. At this point we have the mean intensity within each grid cell and can solve the hydrogen photoionization equation to determine the ionization fraction in each cell. With the ionization fraction and therefore the opacity calculated throughout the grid, we iterate the above procedure, calculating new ionization fractions throughout the grid until convergence is achieved. We typically find that the ionization fractions converge within five iterations.

In order to test the validity of our assumptions, we have tested our code against the spherically symmetric photoionization code of Mathis (1985). The test case we have chosen is the same as that presented by Och et al. (1998). A blackbody ionizing source of $T_{\mathrm{eff}} = 4 \times 10^4$ K and ionizing luminosity $Q(\mathrm{H}^0) = 4.26 \times 10^{49}$ s^{-1} ionizes a region of constant number density $n_{\mathrm{H}} = 100$ cm^{-3}. In our approach, the flux mean cross section for this case is $\bar{\sigma} = 3 \times 10^{-18}$ cm^2. Figure 11 shows the ionization fraction as calculated by our code and by the Mathis code. Even though we have employed many simplifications compared to Mathis' code, our results for hydrogen photoionization (ionization fraction and extent of the ionized region) are in excellent agreement with his.

As a second test case we have compared our code with the two-dimensional "Strömgren volume" calculations of Dove & Shull (1994, their Figs. 1 and 2). They calculated the escape fraction and ionized volumes formed within a three-component galactic disk by point sources of different luminosity. Figure 12 shows the escape fractions calculated by our Monte Carlo code and the analytic escape fractions of Dove & Shull (1994, their eq. [16]). We have plotted the total escape fraction from both sides of the disk, whereas Dove & Shull (1994) showed the escape fraction from one side of the disk. Our Monte Carlo results are in excellent agreement at high luminosities but are systematically lower at low luminosities. This discrepancy arises because we calculate the ionization fraction throughout our grid, whereas the Strömgren volume analysis assumes that the medium is either neutral or fully ionized. In Figure 13 we show three slices through our density grid showing the total number density, ionization fraction, and locations of the regions where photons are absorbed and reemitted as escaping nonionizing radiation. While the Strömgren volume is similar to that shown in Figure 1*d* of Dove & Shull (1994), our calculated neutral fraction of $f \approx 10^{-3}$ provides sufficient opacity to absorb source photons, thereby reducing the escape fraction compared to that of Dove & Shull (1994). In the analysis of Dove & Shull, source photons can escape directly through this ionized "chimney" where they assume a vanishing neutral fraction.

REFERENCES

Abel, T., Norman, M., & Madau, P. 1999, ApJ, 523, 66
Arons, J., & Wingert, D. W. 1972, ApJ, 177, 1
Barkana, R., & Loeb, A. 1999, ApJ, 523, 54
———. 2000, ApJ, 531, 613
Bertschinger, E. 1985, ApJS, 58, 39
Bianchi, S., Ferrara, A., Davies, J. I., & Alton, P. B. 2000, MNRAS, 311, 601
Bianchi, S., Ferrara, A., & Giovanardi, C. 1996, ApJ, 465, 127
Binney, J., & Tremaine, S. 1987, Galactic Dynamics (Princeton: Princeton Univ. Press), 580
Bland-Hawthorn, J., & Maloney, P. R. 1999, ApJ, 510, L33
Boissé, P. 1990, A&A, 228, 483
Bregman, J. N., Kelson, D., & Ashe, G. A. 1993, ApJ, 409, 682
Bryan, G., & Norman, M. 1998, ApJ, 495, 80

Cole, A. A., Wood, K., & Nordsieck, K. H. 1999, AJ, 118, 2292
Couchman, H. M. P., & Rees, M. J. 1986, MNRAS, 221, 53
Dekel, A., & Silk, J. 1986, ApJ, 303, 39
Dey, A., et al. 1998, ApJ, 498, L93
Dove, J. B., & Shull, J. M. 1994, ApJ, 430, 222
Dove, J. B., Shull, J. M., & Ferrara, A. 2000, ApJ, 531, 846
Ferrara, A., Bianchi, S., Cimatti, A., & Giovanardi, C. 1999, ApJS, 123, 437
Ferrara, A., Bianchi, S., Dettmar, R., & Giovanardi, C. 1996, ApJ, 467, L69
Gnedin, N. 2000, ApJ, 535, 530
Gunn, J. E., & Peterson, B. A. 1965, ApJ, 142, 1633
Haiman, Z., Abel, T., & Rees, M. J. 2000, ApJ, 534, 11
Haiman, Z., & Loeb, A. 1997, ApJ, 483, 21
———. 1998, ApJ, 503, 505
———. 1999, ApJ, 521, L9
Haiman, Z., Rees, M., & Loeb, A. 1997, ApJ, 476, 458 (erratum 484, 985)
Haiman, Z., & Spaans, M. 1999, ApJ, 518, 138
Hoopes, C. G., Walterbos, R. A. M., & Rand, R. J. 1999, ApJ, 522, 669
Hu, E. M., Cowie, L. L., & McMahon, R. G. 1998, ApJ, 502, L99
Hu, E. M., McMahon, R. G., & Cowie, L. L. 1999, ApJ, 522, L9
Hurwitz, M., Jelinsky, P., & Dixon, W. 1997, ApJ, 481, L31
Kennicutt, R. C. 1998, ApJ, 498, 541
Koratkar, A., & Blaes, N. 1999, PASP, 111, 1
Laor, A., & Draine, B. T. 1993, ApJ, 402, 441
Leitherer, C., et al. 1999, ApJS, 123, 3
Leitherer, C., Ferguson, H. C., Heckman, T. M., & Lowenthal, J. D. 1995, ApJ, 454, L19
Lucy, L. B. 1999, A&A, 344, 282
Madau, P. 1999, in AIP Conf. Proc. 470, After the Dark Ages: When Galaxies Were Young, ed. S. S. Holt & E. P. Smith (New York: AIP), 299
Madau, P., Haardt, F., & Rees, M. J. 1999, ApJ, 514, 648
Madau, P., & Shull, J. M. 1996, ApJ, 457, 551
Magorrian, J., et al. 1998, AJ, 115, 2285
Mathis, J. S. 1985, ApJ, 291, 247
Miller, W. W., & Cox, D. P. 1993, ApJ, 417, 579
Miralda-Escudé, J., Haehnelt, M., & Rees, M. J. 2000, ApJ, 530, 1
Mo, H. J., Mao, S., & White, S. D. M. 1998, MNRAS, 295, 319
Navarro, J. F., Frenk, C. S., & White, S. D. M. 1997, ApJ, 490, 493
Neufeld, D. A. 1991, ApJ, 370, L85
Nishi, R., & Susa, H. 1999, ApJ, 523, L103
Och, S. R., Lucy, L. B., & Rosa, M. R. 1998, A&A, 336, 301
Omukai, K., & Nishi, K. 1999, ApJ, 518, 64
Osterbrock, D. E. 1989, Astrophysics of Gaseous Nebulae and Active Galactic Nuclei (Mill Valley: University Science Books), 19
Rand, R. J. 1996, ApJ, 462, 712
Razoumov, A. O., & Scott, D. 1999, MNRAS, 309, 287
Reynolds, R. J., Tufte, S. L., Kung, D. T., McCullough, P. R., & Heiles, C. R. 1995, ApJ, 448, 715
Scalo, J. M. 1986, Fundam. Cosmic Phys., 11, 1
Songaila, A. 1997, ApJ, 490, L1
Songaila, A., & Cowie, L. L. 1996, AJ, 112, 335
Spinrad, H., et al. 1998, AJ, 116, 2617
Spitzer, L. 1942, ApJ, 95, 329
Steidel, C. C., Adelberger, K. L., Giavalisco, M., Dickinson, M., & Pettini, M. 1999, ApJ, 519, 1
Stern, D., et al. 2000, ApJ, 533, L75
Tytler, D., et al. 1995, in QSO Absorption Lines, ed. G. Meylan (Heidelberg: Springer), 289
Weymann, R. J., et al. 1998, ApJ, 505, L95
Witt, A. N., & Gordon, K. G. 1996, ApJ, 463, 681
———. 2000, ApJ, 528, 799
Wood, K., & Jones, T. J. 1997, AJ, 114, 1405
Wood, K., & Reynolds, R. J. 1999, ApJ, 525, 799